Biointerphases (2012) 7:62
DOI 10.1007/s13758-012-0062-6

ARTICLE

Investigations on the Secondary Structure of Polypeptide Chains in Polyelectrolyte Multilayers and their Effect on the Adhesion and Spreading of Osteoblasts

Steffi Grohmann · Holger Rothe · Klaus Liefeith

Received: 27 August 2012 / Accepted: 24 September 2012 / Published online: 11 October 2012

Abstract Inspired by the composition of the native extracellular matrix, biomimetic polyelectrolyte multilayers were assembled from polypeptides and the glycosaminoglycan chondroitin sulfate (CS). To investigate whether peptide conformation imposes an effect on the cell biological functions of osteoblasts, the secondary structure was analyzed by *in situ* infra-red and circular dichroism spectroscopy. Multilayers composed of polypeptides and CS reveal a predominantly random coiled conformation and impede osteoblast spreading. On the contrary, polypeptide chains in assemblies of poly-L-lysine and poly-L-glutamic acid (PGA) primarily adopt an intermolecular β sheet structure and reveal an increased area of spread, which consequently supports the proliferation of osteoblasts. When CS is replaced by PGA in mixed multilayers, we observe a structural rearrangement from random coils to β sheets with a concomitant improved cell response. We conclude that polypeptide conformation in biomimetic multilayer assemblies affects osteoblast response by altering the stiffness of the multilayer.

1 Introduction

Polyelectrolyte multilayers (PEM) that are constructed through *Layer by Layer* deposition of oppositely charged polymers have become a powerful tool for tailoring biointerfaces. Over the past 20 years a significant amount of research has been dedicated to the characterization of PEM thin films and their application in life sciences (recently reviewed in [1, 2]). One of the main advantages of *Layer by Layer* assembly is the straightforward technology of immersing substrates into solutions of the selected polyelectrolytes. A wide variety of polyelectrolytes ranging from designed synthetic polymers to naturally derived biopolymers may be employed for film build-up. Biopolymers that can be assembled into multilayer architectures include the following: polypeptides, proteins, nucleic acids and polysaccharides. These biomolecules have been used to construct biomimetic coatings [3–6]. The resulting biomimetic PEM films are of special interest for coating dental and orthopedic implants, particularly when they contain components of the native extracellular matrix of bone. Glycosaminoglycan chondroitin sulfate (CS) is one of the most ubiquitous polysaccharides of the extra cellular matrix (ECM). CS macromolecules are covalently attached to proteoglycan core proteins in a high density and play a key role in tissue metabolism. CS supports the biomineralization process [7–9], and sulfated glycosaminoglycans in general possess binding affinity to growth factors and synergistically support their bioactivity [10]. Enhanced bioactivity can be imposed onto biomimetic PEM films by incorporating sensitive biomolecules, e.g. growth factors, from their aqueous solutions due to the mild coating conditions of the LbL technique [11, 12]. Despite the apparent potential of CS, only a limited number of studies have been dedicated to the characterization and application of PEM assemblies containing CS (just to mention a few [13–21]). This study is the first report on the conformation of the cationic polypeptide poly-L-lysine (PLL) complexed with CS in multilayers. Under fully hydrated conditions, in situ infra-red spectroscopy in the SBSR mode (single beam sample reference) and circular dichroism spectroscopy were employed to characterize the internal structure of $(PLL\text{-}CS)_n$ and $(PLL\text{-}PGA)_n$ films (PGA: poly-L-glutamic

S. Grohmann · H. Rothe · K. Liefeith (✉)
Institute for Bioprocessing and Analytical Measurements Techniques (iba), Heiligenstadt, Germany
e-mail: klaus.liefeith@iba-heiligenstadt.de

acid). Multilayers constructed from two polyanions were characterized with respect to their relative secondary structure composition. This study describes the preparation and analysis of multilayers that display conformational differences in a two dimensionally patterned fashion. We investigated whether the cell morphology and cell density of osteoblasts on PEM films vary with different conformational compositions.

2 Experimental

2.1 Multilayer Preparation

Chemicals and reagents were purchased from Sigma Aldrich (Taufkirchen, Germany) and used without further purification, unless stated otherwise. PEM films were assembled on germanium crystals (Komlas, Berlin, Germany) and/or borosilicate glass discs (diameter 15 mm, B33 glass, Schott, Jena, Germany). The substrates were cleaned with detergents and deionized water prior to film assembly. Glass discs were etched with concentrated nitric acid immediately before the coating procedure. Germanium surfaces were plasma etched for 5 min in order to generate hydroxyl groups and the PEM coating procedure was initiated immediately. PEM films were assembled from poly-L-lysine (PLL, 30–70 kDa), poly-L-glutamic acid (PGA, 50–100 kDa) and chondroitin sulfate (CS, ~63 kDa, from shark cartilage). The polyelectrolytes were dissolved in HEPES/NaCl buffer (25 mM 4-(2-hydroxyethyl)-1-piperazineethanesulfonic acid, 137 mM NaCl, pH 7.4) at a concentration of 1 mg/ml.

Film construction was performed either manually or automatically employing a dipping robot (DR3, Riegler&Kirstein, Germany) as described previously [17]. Briefly, the cleaned substrates were first soaked into the polycation solution (PLL) and left to adsorb for 5 min. Subsequently the samples were soaked into three HEPES/NaCl wash solutions to rinse the surface from unbound polyelectrolytes. The polyanions (PGA or CS) were adsorbed by an incubation for 5 min followed by three rinsing steps. The film construction was performed by repeating these cycles until reaching the desired film architecture. All samples were rinsed in deionized water and air dried in a gentle stream of pressurized air.

2.2 FT-IR Spectroscopy

2.2.1 Spectra Acquisition in SBSR Mode

In order to monitor the secondary structure of thin films, two measuring features are important: (1) sensitivity and (2) fluidic conditions. Thus, PEM film build-up was performed on multiple internal reflection elements (MIRE, trapezoidal germanium (Ge) substrates) that allow for highly sensitive FTIR spectroscopic measurements in the attenuated total reflection mode (ATR). The MIRE was further equipped with a fluidic chamber system that enables a deposition of the polyelectrolytes in flow and an evaluation of the polypeptide conformation under fully hydrated conditions. As schematically depicted in Fig. 1, the fluidic chamber system (four independent compartments) additionally compartmentalizes the MIRE into an upper half that is coated with the PEM (two chambers, one on the upper front side and the other on the upper rear side of the MIRE) and lower half that is continuously rinsed with buffer (two chambers, one on the lower front side and the other on the lower rear side of the MIRE). The IR spectra were recorded in the SBSR mode (single beam sample reference) introduced by Urs Fringeli [22, 23]. Briefly, the sample and reference spectra can be recorded with a minimum delay time by moving the upper and lower half of the MIRE into the IR beam using a standard single beam FTIR instrument. The respective lift-model SBSR mirror attachment (OPTISPEC, Neerach, Switzerland) was mounted on an Equinox 55 equipped with a MCT detector (mercury–cadmium–telluride, nitrogen cooled, Bruker, Karlsruhe, Germany). Measurements were performed on Ge MIRE (50 × 20 × 2 mm^3) with an incident angle of

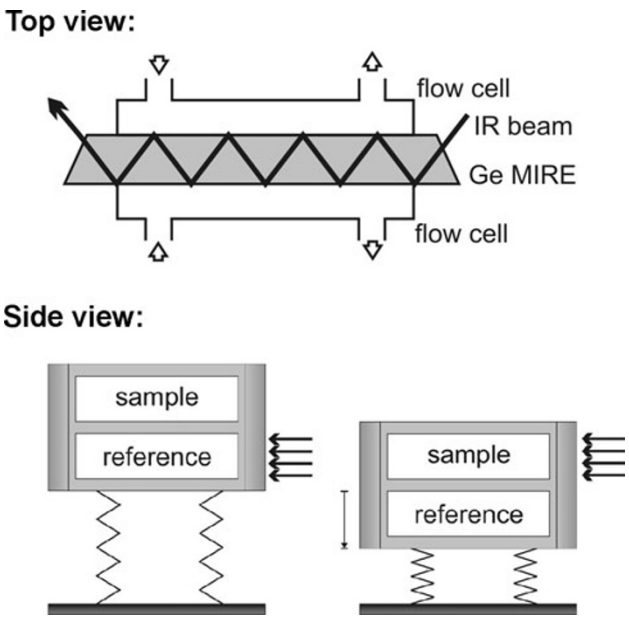

Fig. 1 In situ ATR FTIR with the SBSR set-up. In the *top view* the Ge MIRE (multiple internal reflection element) with its flow cells on each face are displayed. The *side view* schematically displays the vertical movement of the trapezoidal MIRE in a single beam IR instrument to detect the coatings that are deposited in the sample flow cell or the reference flow cell

45° (θ). The number of active reflections N can be determined by applying Eq. (1).

$$N = \frac{l}{\tan\theta \times d} \quad (1)$$

Employing a flow-through cuvette made of Delrin (OPTISPEC, Neerach, Switzerland) the effective length one of the MIRE is limited to 39.7 mm and the resulting number of active reflections is ~19 (for a MIRE thickness d = 2 mm). The Ge MIRE was coated with PEM by sequentially injecting the polycations and polyanions at 0.3 ml/min by means of a peristaltic pump and leaving them to adsorb without flow for 10 min. Subsequently unbound polymers were rinsed off the surface by pumping HEPES/NaCl buffer at flow rate of 0.3 ml/min for 5 min. The reference chambers were charged with HEPES/NaCl buffer (0.3 ml/min) throughout the entire experiment. SBSR FTIR spectra were recorded after the rinsing step without applying flow. Fifty scans were accumulated in a spectral range from 4,000 to 800 cm^{-1} with a resolution of 2 cm^{-1} (zero filling factor two). Experiments were performed at least three times.

2.2.2 Data Processing

The integration of the water bands and the vector normalization of the raw spectra for comparative investigations concerning the secondary structure of the polypeptide chains were performed with the OPUS software package (Bruker, Karlsruhe, Germany). In order to quantify the changes in secondary structure during the build-up of different PEM architectures a partial least square analysis (PLS) based on the principal component analysis (PCA) was performed employing the QUANT 2 package (Bruker, Karlsruhe, Germany, in depth information on multivariate data analysis is described elsewhere [24]). The QUANT 2 model was calibrated with representative spectra for the films $(PLL\text{-}PGA)_{10}$ and $(PLL\text{-}CS)_{10}$. Automatic data processing by the QUANT 2 algorithm comprised vector normalization, first deviation and smoothing (17 points) in the spectral range of 1,599 to 1,702 cm^{-1} (amide I vibration).

2.2.3 FTIR-ATR Microscopy

FTIR-ATR microscopy was performed on patterned PEM films. $(PLL\text{-}CS)_n$ films were prepared on glass substrates and finally incubated with a droplet (~0.1 µl) of PGA solution for 5 min. Subsequently the films were rinsed with buffer and deionized water and dried in a stream of pressurized air. Dried films were analyzed with FITR-ATR microscopy employing a Ge ATR objective (Hyperion, Bruker Optics, Germany). In a scan area of 1.4 × 1.5 mm^2, 72 spectra were recorded. Spectra were analyzed with the Opus 3D software package by integration over defined wave number ranges (specified in the results section).

2.3 CD Spectroscopy

Suprasil quartz substrates (50 × 8.3 × 0.3 mm^3) were cleaned and plasma etched prior to PEM coating. The substrates were dip coated manually as described above. The PEM coated quartz samples were analyzed in phosphate buffer (5 mM, pH 7.4) in a custom made QS cuvette (Hellma, Germany). The rectangular cuvette contains vertical grooves and can hold up to five quartz substrates (optical path 10 mm) [25]. Spectra were recorded in a range from 180 to 260 nm with a resolution of 0.1 nm employing a Jobin–Yvon CD6-Dichrograph (Horiba—Jobin–Yvon, Paris, France).

2.4 Colloidal Force Spectroscopy

Samples with patterned PEM films as described in 2.2.3 were mounted in a fluidic cell and allowed to equilibrate in buffer for 30 min. With the CellHesion AFM (JPK, Berlin, Germany) force maps of 100 × 100 μm^2 were recorded employing cantilevers that were equipped with glass spheres (diameter 11 µm, spring constant was determined to be 63.4 mN/m). For obtaining force distance curves the piezo movement was set to 200 nm (corresponding to an indentation of 30 to 70 nm depending on the stiffness of the coating) after reaching a set point of 1.9 nN. The speed was set to 8 µm/s and after each approach the cantilever was retracted from the polymer film to z = 4 µm above to sample surface before starting a new measurement. The slope of the force distance curves was obtained through a curve fitting procedure and plotted as a stiffness map of the sample surface (all employing the JPK software). Finally, the obtained stiffness values were transformed into Young's moduli employing the modified Hertz sphere model, as described in a previous work [17].

2.5 Cell Biology

All PEM coatings for cell biological analyses were prepared on glass discs and sterilized by UV irradiation. Saos-2 osteoblasts were seeded onto film at a density of 2 × 10^4 cells/cm^2 and cultured in McCoy's 5A medium supplemented with 15 % fetal bovine serum and 1 % penicillin/streptomycin lasting up to 7 days (37 °C, 5 % CO_2, 80 % humidity). After an incubation period of 7 days, cells were enzymatically detached from the surface, stained with trypan blue and counted in a haemocytometer. Cell vitality was assessed as the percentage of

viable cells. Complete trypsinization was verified by phase contrast microscopy.

Fluorescence Microscopy: the culture medium was gently aspirated and the cells were washed with PBS buffer. Fixation was performed by incubation with 4 % paraformaldehyde for 30 min with subsequent rinsing of the fixed cells with PBS buffer. The cytoskeleton was stained with AlexaFluor®594 phalloidin conjugates (Invitrogen, 45 min) and nuclei were counterstained with Hoechst 33258 (Invitrogen, 1 μg/ml in PBS, 10 min). Confocal fluorescence microscopy images were recorded with a LSM 710 (Zeiss, Germany) with appropriate excitation and emission settings.

Scanning Electron Microscopy: samples were fixed with glutaraldehyde, dried by incubating in solutions with increasing alcohol content with subsequent supercritical drying and sputtered with a thin film of gold. SEM analyses were performed on an Evo LS 10 (Zeiss NTS, Oberkochen, Germany).

3 Results and Discussion

3.1 Film Construction

PEM films composed of ten layer pairs (from here on referred to as bilayers) of PLL and a polyanion (PGA and/or CS) were prepared and investigated. In addition to the films containing only one polyanion, two types of coatings were prepared in which the polyanion was switched from PGA to CS and vice versa after five bilayers. After each addition of a polyelectrolyte onto the Ge MIRE in the SBSR flow cell a FTIR spectrum was recorded. Thus, a total of 20 spectra were collected for each investigated PEM film. Figure 2 summarizes the FTIR spectra for the single polyanion films $(PLL\text{-}PGA)_n$ and $(PLL\text{-}CS)_n$ (top and bottom, respectively). In the spectral range of 3,100 to 2,800 cm^{-1} a steady increase corresponding to the methylene moieties of the polymer backbone is observable. Furthermore the absorption band of water (spectral range of 3,600 to 3,100 cm^{-1}) decreases during the coating process. Specific absorptions characteristic for certain moieties of the polyelectrolytes were detected at lower wave numbers. For the $(PLL\text{-}PGA)_n$ films the amide I band (1,600 to 1,700 cm^{-1}), the amide II band ($\sim$1,550 cm^{-1}), a COO^- vibration (1,450 cm^{-1}) and an overtone vibration of the methylene group (1,400 cm^{-1}) were observed (Fig. 2). The spectra of $(PLL\text{-}CS)_n$ films also display amide I, amide II and methylene overtone vibrations. Additionally several absorptions between 1,300 and 900 cm^{-1} were detected indicative of sulfated sugars moieties.

The plot of the amide II absorption over the number of bilayers reveals a non-linear increase of the polypeptide concentration at the MIRE surface for the $(PLL\text{-}PGA)_n$ film (Fig. 3, left panel). The steady decrease in the intensity of the water absorptions indicates shielding of the Ge surface from the bulk water phase due to the PEM film coating. For the $(PLL\text{-}CS)_n$ films two specific absorptions were analyzed. In addition to the amide II vibration accounting for the amount of polypeptide chains on the surface, the sugar/sulfated sugar absorptions were monitored as a measure of the CS concentration (Fig. 3, right panel). Both vibrations become more intense as the number of bilayers increases. As expected the CS absorption does not increase upon the addition of PLL and vice versa.

In an earlier study the growth regimes of both PEM systems were investigated by using reflectometric interference spectroscopy [17]. Both revealed a non-linear increase in the optical film thickness with a higher growth rate for $(PLL\text{-}PGA)_n$ films. The ATR-FTIR spectra underline the non-linear growth of both films and support the steeper increase in film growth of the $(PLL\text{-}PGA)_n$ multilayer. According to the "in and out diffusion model" for exponential film growth this difference may be attributed to the different degrees of diffusibility of PLL chains in PEMs when complexed with PGA or CS [26].

In some cases the PLL specific absorbance decreases upon CS adsorption for films composed of more than eight bilayers. This finding is indicative of a reduced PEM stability for $(PLL\text{-}CS)_n$ with partial film erosion, also referred to as overshooting phenomena [27, 28].

3.2 Polypeptide Conformation

A difference in the shape of the respective amide I bands is obvious from the FTIR spectra for $(PLL\text{-}PGA)_{10}$ and $(PLL\text{-}CS)_{10}$ (Fig. 4a). The shape and exact position of the amide I band allows for an estimation of the secondary structure of the polypeptide chains [29]. A broad band with a maximum around 1,644 cm^{-1} was observed for $(PLL\text{-}CS)_{10}$ films indicating that the PLL chains in this PEM assembly adopt a predominantly random coiled conformation. In the FTIR spectra of the $(PLL\text{-}PGA)_{10}$ films two additional bands at $\sim$1,610 and 1,690 cm^{-1} are detectable. These signals indicate the formation of a β sheet structure by the polypeptide chains (PLL and/or PGA) in this film. Interestingly, the $(PLL\text{-}PGA)_{10}$ spectra resemble data obtained from amyloidal proteins/peptides.

The distinct shift of the amide I vibration from 1,630 to 1,610 cm^{-1} corresponds to the presence of *inter*molecular β sheets as opposed to an *intra*molecularly paired β structure [30]. Thus, building PEM films from PLL and PGA leads to the formation of inter-molecular β sheets (IMβS), which is in agreement with results of previous reports [31, 32].

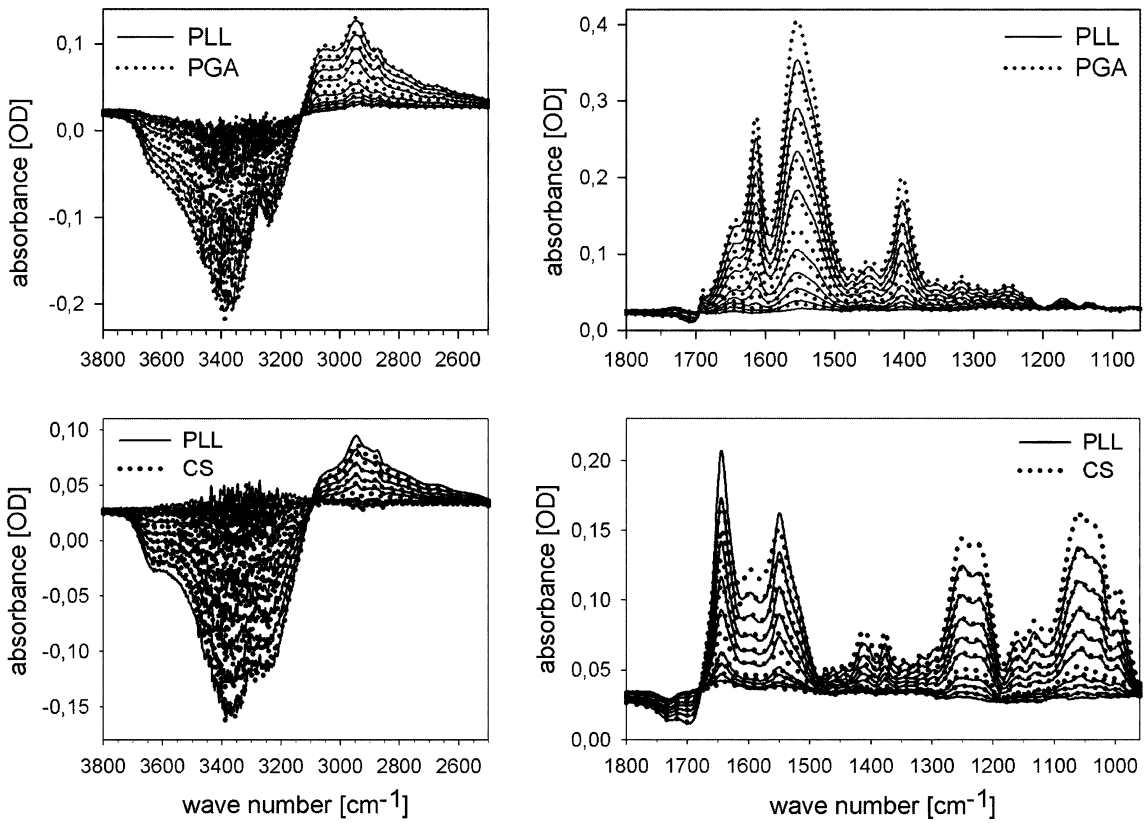

Fig. 2 FTIR spectra of PEM films recorded in the SBSR mode, *top panel* $(PLL\text{-}PGA)_n$ and *bottom panel* $(PLL\text{-}CS)_n$ films

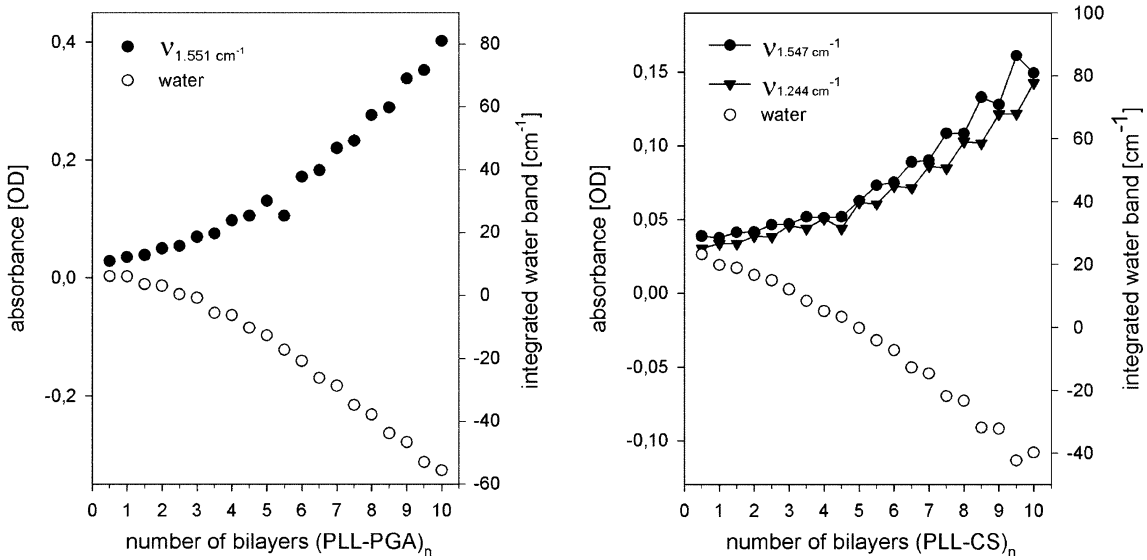

Fig. 3 Evolution of specific IR vibrations with the number of bilayers for $(PLL\text{-}PGA)_n$ films (*left*) and $(PLL\text{-}CS)_n$ films (*right*). Bands around 1,550 cm^{-1} correspond to amide II vibrations and the 1,244 cm^{-1} band corresponds to CS moieties

Circular dichroism spectroscopy was performed to validate the secondary structure evaluations that were obtained by means of FTIR spectroscopy. CD spectra of native (not dried) PEM films on quartz substrates were recorded and compared (Fig. 4, panel B). The data for $(PLL\text{-}CS)_n$ films reveal a negative ellipiticity that converges to the X-axis at $\sim$215 nm that is characteristic for polypeptide chains in a random coiled conformation. Only

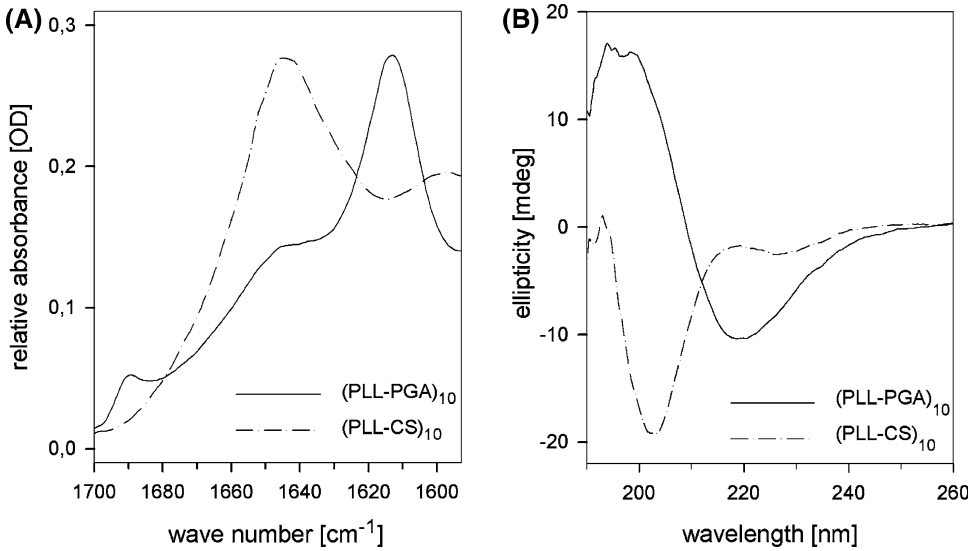

Fig. 4 Amide I absorptions recorded with **a** FTIR and **b** CD spectroscopy data for $(PLL\text{-}PGA)_n$ films (*solid lines*) and $(PLL\text{-}CS)_n$ films (*dashed lines*)

minor contributions of other secondary structure elements like α and β conformations are expected to account for the recorded CD spectra. The CD spectra of $(PLL\text{-}PGA)_n$ films in buffer reveal similar negative π–π^* transitions at $\sim$220 nm and positive n-π^* transitions at 202 nm like they were observed for PLL-PGA complexes in solution [33]. We attributed the dichroitic maxima and minima to the high content of β structure. Whether the β sheets in $(PLL\text{-}PGA)_n$ films are formed between single or multiple polypeptide chains (intra- and intermolecular, respectively) cannot be evaluated from CD spectroscopy. The CD spectra provide further evidence supporting the hypothesis that the polypeptide chains adopt a predominantly random coiled structure in $(PLL\text{-}CS)_n$ films and a predominantly β-structural conformation in $(PLL\text{-}PGA)_n$ films.

Both PLL and PGA chains are known to adopt random coiled secondary structures in a physiological milieu (pH 7.4, isotonic salt concentrations) [29]. It is well known from the literature that it is possible to induce conformational changes for polypeptides like PLL and PGA in solution. By varying the pH, temperature and salt ions of the solution a transition of the polypeptide conformation from random coiled to α helices, β sheets and intermolecular β sheets was observed [29]. When these folded polypeptides are adsorbed onto material surfaces their secondary structure is usually retained [31, 34, 35]. The results obtained in this study for PLL chains in $(PLL\text{-}CS)_n$ assemblies, i.e. that they retain their predominantly random coiled conformation, are consistent with recent reports on the conformation of PLL chains in $(PLL\text{-}PAA)_n$ assemblies [36] and PGA chains in $(PAH\text{-}PGA)_n$ assemblies [31] (PAA: poly-L-aspartic acid, PAH: poly-allylamine hydrochloride). Currently, IMβS formation in multilayers was reported for the following polypeptide pairs: PLL/PGA, poly-D-lysine/PGA and poly-L-ornithine/PGA [37]. The self assembly of $(PLL\text{-}PAA)_n$ and $(PLL\text{-}PGA)_n$ into completely different conformations despite sharing similar chemical features is striking. A possible explanation for the formation of IMβS structure for $(PLL\text{-}PGA)_n$ assemblies could be due to the longer side chain of PGA as compared to PAA, indicating that hydrophobic interactions between the side chains of the polypeptide may contribute to the stability of the conformation. However, although ornithine's (an amino acid not involved in protein synthesis) side chain is one methylene group shorter than lysine its polymer readily forms IMβS structures with PGA. Alternatively, the lower pK_a value (PAA: $pK_a = 5.4$, PGA: $pK_a = 4.5$, [38]) and consequently the higher degree of ionization may affect the IMβS formation and stability indicating that salt bridges between PGA and PLL side chains are critically important. In this case, the shorter length of the PAA side chain may sterically hinder the formation of ionic bonds with the corresponding amides of the polycation. PLL and poly-L-ornithine possess similar pK values of 10.4 and 10.1, respectively [39].

To estimate the different contributions of secondary structure components to the entire structure more quantitatively, a QUANT 2 calibration model was defined and the evolution of the conformation was evaluated with respect to the film architecture. The reference spectra of $(PLL\text{-}CS)_{10}$ films with a predominant random coiled structure and $(PLL\text{-}PGA)_{10}$ films with a predominant intermolecular β structure were defined as conformation A and conformation B, respectively. For each of the investigated ten bilayer films the 20 collected FTIR spectra were analysed with respect to their content of conformation A and conformation B. Figure 5 displays the evolution of the secondary structure composition (expressed as the relative content of conformation B) of the polypeptide chains as determined from the QUANT 2 analyses. During the first

few deposited layers (up to two layer pairs) the surface concentration on the MIRE is low, resulting in high signal to noise ratio. However, as the concentration of the polyelectrolytes (PE) on the surface increases the quality of the spectra improves and thus the QUANT 2 analyses results are more reliable. For the $(PLL\text{-}PGA)_n$ films an increase in conformation B was determined for the deposition over the first few double layers. After this lag phase, consistently steady contents of conformation B for the PLL and PGA chains were detected. Interestingly, the increase in β structure is more pronounced when PGA is adsorbed, while PLL causes an increase in the random coiled structure. The content of conformation B cyclically increases and decreases upon PGA and PLL adsorption, respectively. Noteworthy, the gain in IMβS structure does not imply that the total amount of random coiled polypeptide chains is reduced upon PGA adsorption, as was observable from the respective difference spectra. On the other hand, the decrease in conformation B after PLL deposition does not involve the destruction of intermolecular β sheets. For the second type single polyanion multilayer; $(PLL\text{-}CS)_n$; a stable random coiled structure (corresponding to 0 % conformation B) develops during the film build-up.

After investigating the structure of PEM films composed of one polyanion the effects of changing the polyanion during film construction was analyzed. When CS was adsorbed onto a $(PLL\text{-}PGA)_5$-PLL film an effect on the secondary structure was observed (Fig. 5). With each deposited bilayer of (PLL-CS) the content of conformation B decreases, and consequently the number of polypeptide chains in random coiled conformations increases. After an addition of 5 bilayers (PLL-CS) onto a $(PLL\text{-}PGA)_5$ basis approximately 25 % of the polypeptide chains are in conformation A and 75 % in conformation B. The intensity of the IMβS structure does not decrease while the signal for random coiled conformation rises (as judged from difference spectra after PE adsorption), this suggests that a bizonal film structure results due to the change in the polyanion from PGA to CS during PEM assembly. The first zone (in proximity to the substrate surface) is predominantly composed of intermolecular β structure while the second zone (towards the film–buffer interface) is characterized by chains in random coiled conformation.

An even more pronounced effect on the film structure was observed when the polyanion was switched from CS to PGA. Upon the adsorption of the first PGA layer onto $(PLL\text{-}CS)_5$-PLL a significant structural reorganisation occurred (Fig. 5). PGA deposition caused a rise in the content of conformation B from 0 % to more than 80 %. After the deposition of five bilayers of PLL-PGA on top of a $(PLL\text{-}CS)_5$ film a secondary structure that closely resembles the conformation of a pure $(PLL\text{-}PGA)_{10}$ assembly (i.e. 100 % conformation B) was obtained. As observed for the construction of pure $(PLL\text{-}PGA)_n$ films, the adsorption of PGA causes a dramatic increase in β sheet structure when compared to the adsorption of PLL.

The difference spectrum after PGA adsorption reveals a certain loss of CS chains either due to desorption of soluble PLL-CS complexes or through the substitution of CS chains by PGA. The fact that CS chains are not completely removed from the multilayer may be explained by the structural model that Abdelkebir et al. [13] recently

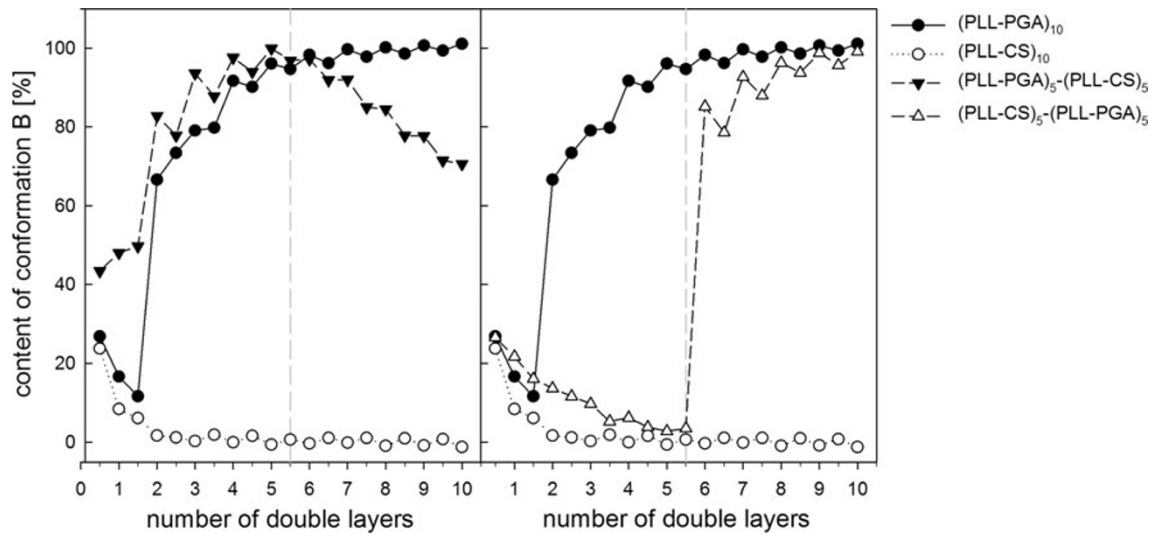

Fig. 5 Comparative investigations on the secondary structure content with respect to the film architecture. The evolution of the polypeptide chain conformations during film build-up for $(PLL\text{-}PGA)_{10}$ (*filled circles*) and $(PLL\text{-}CS)_{10}$ (*empty circles*) is compared to $(PLL\text{-}PGA)_5$–$(PLL\text{-}CS)_5$ (*filled triangles*, *left panel*) and $(PLL\text{-}CS)_5$–$(PLL\text{-}PGA)_5$ (*open triangles*, *right panel*). The content of conformation B was determined from the amide I absorptions employing QUANT 2 analyses. Representative plots of three measurements are displayed

proposed for $(PLL\text{-}CS)_n$ multilayers. This type of PEM film is proposed to consist of a loosely assembled surface zone and a densely packed (ionically cross-linked) zone in proximity to the substrate interface. The extent of hydration of the loose surface zone is sufficiently high, that the CS chains may be more prone to a replacement with PGA chains and/or film erosion via the formation of soluble polyelectrolyte complexes (PECs). The CS chains in the deeper zone, which is proposed to display a dense network of ionic cross-links, may be less susceptible to substitution via detachment processes. The CS chains that remain tightly bound to the PLL molecules in the dense zone are postulated to account for the sugar and sulfate vibrations in the IR spectrum of the $(PLL\text{-}CS)_5$-$(PLL\text{-}PGA)_5$ mixed multilayers.

Only few studies have been dedicated to the influence of using multiple polyanions (or polycations) for film construction on the resulting secondary structure of the assembly [36, 37, 40]. Debreczeny et al. [36] assembled films from PLL complexed with different mixtures of PGA and poly-L-aspartic acid (PAA), while in the present study the effect of changing the polyanion was investigated. While $(PLL\text{-}PAA)_n$ assemblies were characterized by a mainly random coiled structure, the addition of PGA to the PAA solution during build-up induced the formation of IMβS in the PEM film. The content of IMβS strongly increased when the concentration of PGA was raised. In a similar experiment, the same group deposited PGA onto $(PLL\text{-}PAA)_n$ films and revealed a substitution of the PAA chains by PGA with a concomitant formation of IMβS [40]. We suggest that the mechanisms by which PGA displaces PAA in $(PLL\text{-}PAA)_n$ assemblies [40] and CS in $(PLL\text{-}CS)_n$ films (results of this study) are similar. Apparently, PGA breaks the bonds between PLL and CS (or PAA) and compels the PLL backbone into a β pleated sheet. The formation of the intermolecular β sheet seems to be an energetically favourable process and the resulting structure is extremely stable. This remarkable stability towards pH changes (pH range 4 to 10.5 [37]), temperature and drying-rehydration cycles [41, 42] is likely due to the multitude of hydrogen bonds between adjacent backbone carbonyl and amide, ion pairings of the charged side chains and potentially hydrophobic interactions between the methylene moieties of the PLL and PGA side chains. Only the exposure to extremely acidic buffers induces conformational changes and yields the formation of a porous film structure [33]. Albeit, the $(PLL\text{-}PGA)_n$ assemblies are susceptible to chain substitution of PGA by stronger polyelectrolytes like poly(styrene sulfonate) that also breaks the IMβS structure [37].

3.3 Cell Biological Evaluation

In order to investigate the effect that the secondary structure imposes on the adhesion and spreading of osteoblasts, coatings that display different amounts of conformation B in the range of ~70 to 100 % were prepared and seeded with cells. The mixed multilayers were additionally classified according to the polyanion that is exposed on the film surface (Table 1). The single polyanion multilayers of CS (0 % conformation A) and PGA (100 % conformation B) served as references for this experiment.

In addition to a characterisation of the cell morphology after 4 days of culture, the cell biological analysis evaluated cell density and viability after an incubation time of 7 days. The cell density on pure CS films is extremely low, reaching less than 20 % compared to the uncoated glass surface (Fig. 6c). An improvement of the cell count on the respective films is observed when the content of conformation B exceeds 70 %. The cell count on the sample surfaces generally increased with an increasing content of conformation B in the PEM films. Interestingly, there was an apparent difference in cell performance in dependence of the exposed terminating polyanion layer for mixed multilayers with comparable contents of conformation B (84 and 90 %). The cell count on CS terminating multilayers was approximately 20 to 30 % lower than the cell count on the respective films with a top layer of PGA. No influences on the cell vitality were observable for any of the investigated samples (data not shown).

Table 1 Summary of the nomenclature, estimated secondary structure composition and architecture for the samples that were characterized in cell biological experiments

Sample	Estimated content of conformation B (%)	Top layer	Architecture
CS 70 %	70	CS	$(PLL\text{-}PGA)_5$–$(PLL\text{-}CS)_5$
CS 84 %	84	CS	$(PLL\text{-}PGA)_5$–$(PLL\text{-}CS)_3$
CS 90 %	90	CS	$(PLL\text{-}PGA)_5$–$(PLL\text{-}CS)_2$
PGA 84 %	84	PGA	$(PLL\text{-}CS)_5$–$(PLL\text{-}PGA)_1$
PGA 90 %	90	PGA	$(PLL\text{-}CS)_5$–$(PLL\text{-}PGA)_2$
PGA 100 %	100	PGA	$(PLL\text{-}CS)_5$–$(PLL\text{-}PGA)_5$
CS, solely	0	CS	$(PLL\text{-}CS)_{10}$
PGA, solely	100	PGA	$(PLL\text{-}PGA)_{10}$

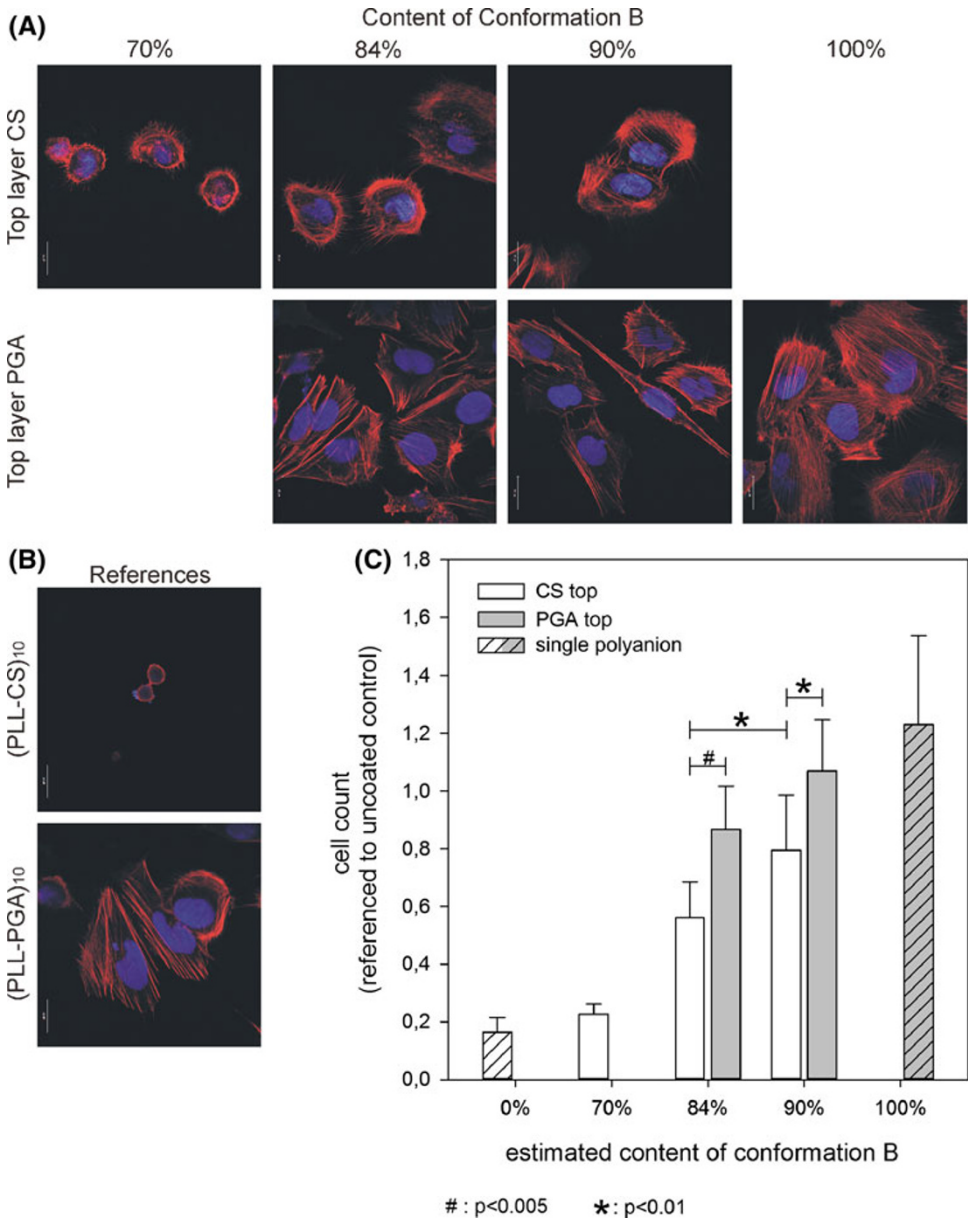

Fig. 6 Cell biological analyses on multilayers constructed from single and multiple polyanions with respect to the conformation of polypeptide chains in the film expressed as the percentage of conformation B. All PEM films were prepared with a top layer of the respective polyanion (CS or HEP). **a**, **b** Cell morphology of SaOs osteoblasts cultured on the films for 4 days (*red* actin cytoskeleton stained with a phalloidin conjugate, *blue* nuclei stained with Hoechst 33258, *scale bar* 20 μm). **c** Cell count on samples that were incubated with osteoblasts for 7 days referenced to uncoated glass controls (data are presented as mean ± SD for nine samples per modification in three independent experiments, *p* values for significantly different pairs are indicated)

The cell morphological analyses provided corresponding results (Fig. 6a). While the osteoblasts do not spread on films with a content of conformation B less than 70 %, the area of cell spread increased significantly when the content of conformation B was raised. In accordance with the cell count data the osteoblasts that were cultured on mixed multilayers with PGA as the top layer displayed a more extended morphology than cells that were seeded onto CS terminated films. While cells on PGA layers are predominantly well spread, the actin cytoskeleton is poorly developed when the osteoblasts are seeded onto CS top layer films, especially when they contain a high content of random coiled structure. As described in a previous study and by other groups there is a strong correlation between proliferation capacity and the spreading area of substrate dependent cells like osteoblasts (Fig. 6c) [17, 43, 44].

Given that the cell biological effect cannot solely be due to the physico-chemical differences between CS and PGA, the results of the cell culture experiments indicate that osteoblasts preferentially adhere and proliferate on polypeptide films with an intermolecular β structure. In contrast conformation A, a predominantly random coiled composition of polypeptide chains, poorly supports cell spreading and proliferation. In a previous study, we demonstrated that the surface charge (zeta potential) and the surface roughness (by means of AFM) are comparable for $(PLL\text{-}CS)_{10}$ and $(PLL\text{-}PGA)_{10}$ films. A prominent dissimilarity was detected for the stiffness of these multilayers [17]. The

mechanical properties of PEM assemblies may well be correlated to the conformation of their polypeptide chains. Random coiled chains are usually loosely assembled with a high degree of flexibility resulting in a low mechanical stiffness. The low stiffness is a result of the high degree of swelling caused by the CS chains. On the contrary, the backbones of polypeptide chains that self-assemble into intermolecular β sheets are tightly packed and their conformation is stabilized by a multitude of hydrogen bonds (peptide backbone) and salt bridges (side chains). This tightly packed polymer network consequently displays an elevated stiffness. Additionally, the hydration with water molecules may be sterically hindered and reduce the swelling of the films.

The cell biological investigations on mixed multilayers further reveal that the PEM film conformation is not sensed as a property of a homogeneous 3D-volume phase by the cells, since a difference in cell density was observed on PGA compared to CS terminated films. These results support the hypothesis that $(PLL\text{-}PGA)_n$–$(PLL\text{-}CS)_x$ multilayers display a bizonal structure with distinct polypeptide conformations. When the number of CS bilayers x increases the superficial, random coiled zones covers the tightly packed underlying $(PLL\text{-}PGA)_n$. Consequently, both the content of conformation B in the film volume and the conformation of the surface exposed layers affect the cell response. When the top layers of the mixed multilayers with similar content of conformation B are composed of random coiled chains, their inherent mechanical softness negatively interferes with cell spreading and proliferation.

3.4 Patterned Multilayers

A patterning of the multilayer coating was achieved by incubating $(PLL\text{-}CS)_{20}$ films with droplets of the PGA coating solution. It is important to note that the adsorption of the negatively charged PGA was performed on multilayers with a top layer of negatively charged CS (and not the positively charged PLL). The resulting patterned multilayer films were subsequently characterized by means of FTIR-ATR microscopy, colloidal force microscopy and cell biological investigations (Fig. 7).

FTIR microscopic analyses were performed on dried multilayers with a germanium ATR objective and revealed tremendous conformational rearrangements in the PGA treated areas of the coating. The recorded spectra were integrated with respect to conformation A (1,635–1,700 cm^{-1}), conformation B (1,600 to 1,635 cm^{-1}) and the entire amide I vibration (1,600 to 1,700 cm^{-1}). The maps for the integrated conformation B band display an increase of IMβS from the untreated to the PGA treated area (Fig. 7, panel A, white to grey, respectively).

The IMβS formation is accompanied by a concomitant decrease in conformation A (data not shown). No differences in the total area under the amide I vibration were observed for the scanned area (data not shown). The structural rearrangement into conformation B is accompanied by an impressive increase in film stiffness as assessed with colloidal force spectroscopy in mapping mode (Fig. 7, panel B, black corresponds to soft, white corresponds to more rigid). In relation to the Young's modulus of

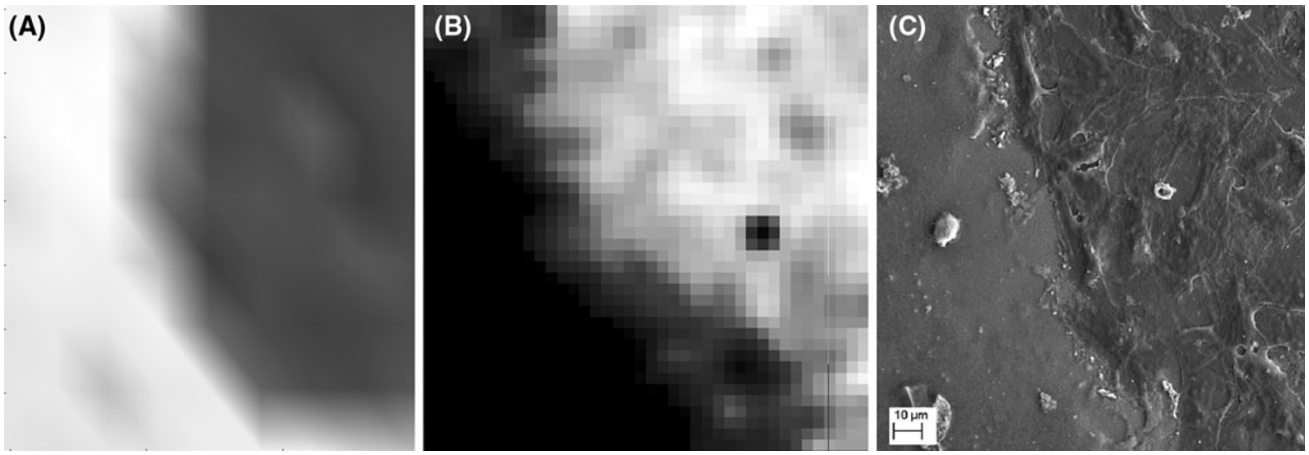

Fig. 7 Characterization of patterned PEM films that were prepared by incubating a droplet of PGA solution onto a preassembled $(PLL\text{-}CS)_{20}$ multilayer on glass. **a** FTIR-ATR microscopy results are presented as integration over the wave number range from 1,600 to 1,635 cm^{-1}. *Color scale* from *white* to *grey* indicates an increase in conformation B (0.0 to 0.6 arbitrary integration units, image size 1.4 mm × 1.5 mm). **b** Colloidal force microscopy map that indicates an increasing stiffness of the PGA treated film area (color scale *white* = 47 pN/nm to *black* = 68 pN/nm, image size (100 µm)^2). **c** SEM image of osteoblasts that were incubated on the patterned PEM films for 7 days (original magnification ×500, *scale bar* 10 µm). A segment of the circular PGA treated area is depicted in the *upper right corner* of each panel

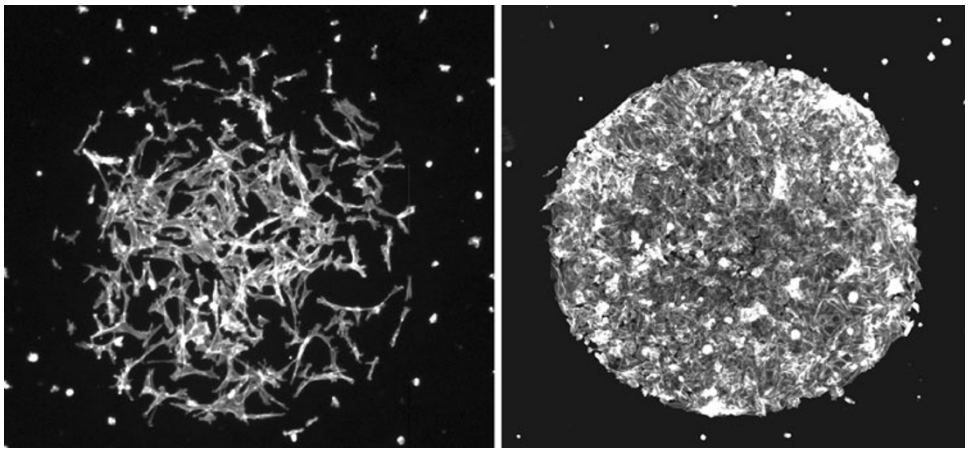

Fig. 8 Cell morphological analyses on patterned multilayers that were prepared by incubating a droplet of PGA solution onto a preassembled $(PLL\text{-}CS)_{20}$ multilayer on glass. Osteoblasts were seeded onto the samples and incubated for 4 and 7 days (*left* and *right*, respectively). Actin cytoskeleton was stained with a phalloidin conjugate, droplet diameter ~ 1 mm

untreated $(PLL\text{-}CS)_n$ films, which was determined to be approximately ~ 9 kPa [17], the elasticity of the PGA treated area was significantly increased to 369 ± 143 kPa (corresponding to a difference in film stiffness of ~ 12 pN/nm, $p < 0.0001$). This stiffness is lower compared to the stiffness of $(PLL\text{-}PGA)_n$ films that was determined to be ~ 700 kPa [17]. In a recent study by Schoeler et al. [45] the effects of the conformation of PE on the multilayers mechanical properties were observed, as well. Films composed of polysaccharides (carrageenan) in an ordered conformation displayed increased stiffness as compared to their respective counterparts that displayed a random conformation.

In the stiffer areas of the patterned coatings, a significantly improved cell spreading was observed and the osteoblasts' proliferation was supported more efficiently than on the untreated areas of the film (Fig. 7, panel C). Cell morphological analyses on osteoblasts that were cultured on the circular patterns for 4 and 7 days further support this hypothesis (Fig. 8). Improved cell spreading in the patterned spots after 4 days results in an elevated proliferation activity (compared to the untreated surface) yielding a confluent monolayer of osteoblasts on the treated areas after 7 days. The cells on the untreated film remain poorly spread and are sparsely distributed. The effect that an increasing PEM film stiffness results in an increased area of spread and proliferation of osteoblast-like cells was previously observed in other studies, as well [17, 44, 46]. The observed structural changes in the PEM film can only be explained by a diffusion of PGA chains into the $(PLL\text{-}CS)_{20}$ assembly passing the electrostatic barrier. A diffusion of polypeptides into and within PEM films has been described already. In a study by Picart et al. [26] the polypeptide PLL diffused into multilayers composed of PLL and the polysaccharide hyaluronan. If PGA was solely deposited as a single layer on top of the CS film the structural and mechanical properties were not likely to have changed to the same degree. The structural rearrangements within the film area that was incubated with the droplet of PGA solution did not only result in a change in polypeptide conformation and in the mechanical film properties. It was also observed that a ring of higher film thickness formed around the created pattern and that the thickness of the PGA treated area decreased. Since it was known from the FTIR experiments that CS chains are in part replaced by PGA molecules, we suggest that the displaced CS material accumulated at the rim of the deposited droplet despite the films being thoroughly rinsed. This circular accumulation is interesting since the PEM film morphology actually resembles a cavity of high osteoblast adhesion and proliferation capacity within an otherwise poorly adhesive substrate. The elevated and soft rim of this cavity may potentially sustain the boundary function and thus retain the adhesion/proliferation patterns for more than 7 days of incubation.

Whether the CS chains are "forced to diffuse" out of the PGA treated film volume and complex "free" PLL chains at the air/buffer/film interface or whether entire soluble PLL-CS complexes are released from the film and accumulated to form the rim, remains speculative. Since we found evidence for a limited diffusion of the PGA chains within the $(PLL\text{-}CS)_{20}$ films and the film thickness decreased in the treated area, a mechanism based on the erosion of soluble PLL-CS complexes seems to be the more plausible explanation. Nevertheless, to understand this phenomenon in more detail further research has to be focused on the patterned films.

4 Conclusion

The layer-by-layer assembly of polypeptides offers the opportunity to control conformational arrangements. Compared to the secondary structure in solution the conformation of the polypeptide chains can either be maintained (as in the case of PLL-CS) or rearranged (as in the

case of PLL-PGA) depending on the choice of the PE pairs. PGA was revealed to be a potent inducer of an intramolecular β pleated structure in both PLL-PGA and in PLL-CS assemblies. The results of this study suggest that there is a correlation between the conformation of polypeptides in the film and the mechanical properties of the coating. PEM films composed of polypeptide chains with a random coiled structure result in rather soft coatings, while similar films that display a high degree of intermolecular β pleated sheets reveal an increased Young's modulus. Especially for cells that obey to the rules of durotaxis, this increase in the film's β structure content strongly supports cell spreading and an increased cell density after 7 days was observed. In addition to the effects on the film's mechanical properties the secondary structure of the PEM may also affect the conformation of proteins that adsorb to its surface [40]. It was recently discussed in a study by Ball and coworkers whether the polypeptide conformation may influence the nucleation kinetics of calcium phosphates on PEM [47]. An example of how the formation of IMβS may be harnessed in (nano)biotechnological applications was recently demonstrated by Higashi et al. [48] who utilized PGA conjugation to nanoparticles to assist a well-ordered assembly of the nanoparticles on PEM templates. The capability of PGA to induce β pleated sheets in predefined areas can be exploited to create biomimetic coatings with patterned biological functions which would be useful for future applications in the fields of chip based co-culture approaches, biotechnology and life sciences.

Acknowledgments The authors thank Martina Lackner and Christina Biermann for technical assistance. Financial support for parts of this study was provided by the Deutsche Forschungsgemeinschaft (DFG) and the German Israeli Foundation (GIF), and is gratefully acknowledged.

References

1. Gribova V, Auzely-Velty R, Picart C (2011) Chem Mater 24(5):854–869. doi:10.1021/cm2032459
2. El khouri RJ, Szamocki R, Sergeeva Y, Felix O, Decher G (2011) Multifunctional layer by layer architectures for biological applications. In: Knoll W, Advincula RC (eds) Functional polymer films, vol 1. Wiley-VCH, Weinheim, pp 11–71
3. Fu J, Ji J, Yuan W, Shen J (2005) Biomaterials 26(33):6684–6692. doi:10.1016/j.biomaterials.2005.04.034
4. Johansson JÅ, Halthur T, Herranen M, Söderberg L, Elofsson U, Hilborn J (2005) Biomacromolecules 6(3):1353–1359. doi:10.1021/bm0493741
5. Thierry B, Winnik FM, Merhi Y, Silver J, Tabrizian M (2003) Biomacromolecules 4(6):1564–1571. doi:10.1021/bm0341834
6. Abdelkebir K, Gaudière F, Morin-Grognet S, Coquerel G, Atmani H, Labat B, Ladam G (2011) Langmuir 27(23):14370–14379. doi:10.1021/la2033109
7. Embery G, Hall R, Waddington R, Septier D, Goldberg M (2001) Crit Rev Oral Biol Med 12(4):331–349. doi:10.1177/10454411010120040401
8. Jiang H, Liu X-Y, Zhang G, Li Y (2005) J Biol Chem 280(51):42061–42066. doi:10.1074/jbc.M412280200
9. Schneiders W, Reinstorf A, Ruhnow M, Rehberg S, Heineck J, Hinterseher I, Biewener A, Zwipp H, Rammelt S (2008) J Biomed Mater Res, Part A 85(3):638–645. doi:10.1002/jbm.a.31611
10. Hudalla GA, Murphy WL (2011) Adv Funct Mater 21(10):1754–1768. doi:10.1002/adfm.201002468
11. Macdonald ML, Rodriguez NM, Shah NJ, Hammond PT (2010) Biomacromolecules 11:2053–2059
12. Macdonald ML, Samuel RE, Shah NJ, Padera RF, Beben YM, Hammond PT (2011) Biomaterials 32(5):1446–1453. doi:10.1016/j.biomaterials.2010.10.052
13. Abdelkebir K, Gaudiere F, Morin-Grognet S, Coquerel G, Labat B, Atmani H, Ladam G (2011) Soft Matter 7(19):9197–9205. doi:10.1039/c1sm05800b
14. Almodovar J, Place LW, Gogolski J, Erickson K, Kipper MJ (2011) Biomacromolecules 12(7):2755–2765. doi:10.1021/bm200519y
15. Crouzier T, Picart C (2009) Biomacromolecules 10(2):433–442. doi:10.1021/bm8012378
16. Etienne O, Schneider A, Taddei C, Richert L, Schaaf P, Voegel JC, Egles C, Picart C (2005) Biomacromolecules 6(2):726–733. doi:10.1021/bm049425u
17. Grohmann S, Rothe H, Frant M, Liefeith K (2011) Biomacromolecules 12(6):1987–1997. doi:10.1021/bm200258q
18. Macdonald ML, Rodriguez NM, Shah NJ, Hammond PT (2010) Biomacromolecules 11(8):2053–2059. doi:10.1021/bm100413w
19. Richert L, Lavalle P, Payan E, Shu XZ, Prestwich GD, Stoltz JF, Schaaf P, Voegel JC, Picart C (2004) Langmuir 20(2):448–458. doi:10.1021/la035415n
20. Tezcaner A, Hicks D, Boulmedais F, Sahel J, Schaaf P, Voegel JC, Lavalle P (2006) Biomacromolecules 7(1):86–94. doi:10.1021/bm0506134
21. Wood KC, Boedicker JQ, Lynn DM, Hammond PT (2005) Langmuir 21(4):1603–1609. doi:10.1021/la0476480
22. Fringeli UP (1992) CHIMIA Int J Chem 46(5):200–214
23. Baurecht D, Reiter G, Hassler N, Schwarzott M, Fringeli UP (2005) CHIMIA Int J Chem 59(5):226–235
24. Beebe KR, Kowalski BR (1987) Anal Chem 59(17):1007–1017
25. Hylton DM, Shalaby SW, Latour RA (2005) J Biomed Mater Res, Part A 73A(3):349–358. doi:10.1002/jbm.a.30295
26. Picart C, Mutterer J, Richert L, Luo Y, Prestwich GD, Schaaf P, Voegel J-C, Lavalle P (2002) Proc Nat Acad Sci 99(20):12531–12535. doi:10.1073/pnas.202486099
27. Grohmann S, Rothe H, Eisenhuth S, Hoffmann C, Liefeith K (2011) Biointerphases 6(2):54–62. doi:10.1116/1.3589176
28. Sukhishvili SA, Kharlampieva E, Izumrudov V (2006) Macromolecules 39(26):8873–8881
29. Susi H, Timasheff SN, Stevens L (1967) J Biol Chem 242(23):5460–5466
30. Zandomeneghi G, Krebs MR, McCammon MG, Fandrich M (2004) Protein Sci 13(12):3314–3321. doi:10.1110/ps.041024904
31. Boulmedais F, Ball V, Schwinte P, Frisch B, Schaaf P, Voegel JC (2003) Langmuir 19(2):440–445
32. Itoh K, Tokumi S, Kimura T, Nagase A (2008) Langmuir 24(23):13426–13433. doi:10.1021/la8015832
33. Z-l Zhi, Haynie DT (2004) Macromolecules 37(23):8668–8675. doi:10.1021/ma049136y
34. Müller M, Ouyang W, Keßler B (2007) Int J Polym Anal Charact 12(1):35–45. doi:10.1080/10236660601064872

35. Müller M, Ouyang W, Keßler B (2010) Spectrochim Acta Part A Mol Biomol Spectrosc 77(4):709–716. doi:10.1016/j.saa.2010.05.032
36. Debreczeny M, Ball V, Boulmedais F, Szalontai B, Voegel JC, Schaaf P (2003) J Phys Chem B 107(46):12734–12739
37. Boulmedais F, Bozonnet M, Schwinté P, Voegel JC, Schaaf P (2003) Langmuir 19(23):9873–9882. doi:10.1021/la0348259
38. Gutierrez E, Miller TC, Gonzalez-Redondo JR, Holcombe JA (1999) Environ Sci Technol 33(10):1664–1670. doi:10.1021/es981166r
39. Chaudhuri SR, Yang JT (1968) Biochemistry 7(4):1379–1383. doi:10.1021/bi00844a020
40. Pilbat A-M, Ball V, Schaaf P, Voegel J-C, Szalontai B (2006) Langmuir 22(13):5753–5759. doi:10.1021/la060454v
41. Zhang L, Haynie DT (2007) Biomacromolecules 9(1):185–191. doi:10.1021/bm700967k
42. Zhang L, Zhao W, Rudra JS, Haynie DT (2007) ACS Nano 1(5):476–486. doi:10.1021/nn700267g
43. Chen CS, Mrksich M, Huang S, Whitesides GM, Ingber DE (1997) Science 276(5317):1425–1428
44. Richert L, Engler AJ, Discher DE, Picart C (2004) Biomacromolecules 5(5):1908–1916. doi:10.1021/bm0498023
45. Schoeler B, Delorme N, Doench I, Sukhorukov GB, Fery A, Glinel K (2006) Biomacromolecules 7(6):2065–2071. doi:10.1021/bm060378a
46. Schneider A, Francius G, Obeid R, Schwinté P, Hemmerlé J, Frisch B, Schaaf P, Voegel JC, Senger B, Picart C (2006) Langmuir 22(3):1193–1200
47. Ball V, Michel M, Boulmedais F, Hemmerle J, Haikel Y, Schaaf P, Voegel JC (2005) Cryst Growth Des 6(1):327–334. doi:10.1021/cg050044p
48. Higashi N, Takagi T, Koga T (2010) Polym J 42(1):95–99. doi:10.1038/pj.2009.311